ISSN 1990-7931, Russian Journal of Physical Chemistry B, 2024, Vol. 18, No. 3, pp. 805–820. © Pleiades Publishing, Ltd., 2024.

CHEMICAL PHYSICS OF NANOMATERIALS

Competitive Intracellular Hydrogen-Nanocarrier Among Aluminum, Carbon, or Silicon Implantation: a Novel Technology of Eco-Friendly Energy Storage using Research Density Functional Theory

F. Mollaamin*, **

Department of Biomedical Engineering, Faculty of Engineering and Architecture, Kastamonu University, Kastamonu, Turkey

**e-mail: fmollaamin@kastamonu.edu.tr*

***e-mail: smollaamin@gmail.com*

Received December 19, 2023; revised January 5, 2024; accepted January 22, 2024

Abstract—This work proposes that metallic, nonmetallic, metalloid as a semiconductor can be examined through doping on the pristine boron nitride nanocell (B_5N_{10}_NC) for ameliorating the adsorption potential of the nanosurface towards designing the energy storage device. Hydrogen adsorption by using X (X=Al, C, Si)-doped B_5N_{10}_NC have been investigated using density functional theory. The partial density of states can evaluate a determined charge assembly between hydrogen molecules and X–B_4N_{10}_NC which indicates the competition among dominant complexes of metallic (Al), nonmetallic (C), metalloid/semiconductor (Si). Based on nuclear quadrupole resonance analysis, carbon-doped on B_5N_{10}_NC has shown the lowest fluctuation in electric potential and the highest negative atomic charge on doping atoms including C, Si, and Al including 0.1167, 1.0620, and 1.1541 coulomb in H_2@C–B_4N_{10}_NC, H_2@Si–B_4N_{10}_NC, and H_2@Al–B_4N_{10}_NC, respectively, can be an appropriate option with the highest tendency for electron accepting in the adsorption process. Furthermore, the reported results of nuclear magnetic resonance spectroscopy have exhibited that the yield of electron accepting for doping atoms on the X–B_4N_{10}_NC through H_2 adsorption can be ordered as: Si ≈ Al > C that exhibits the strength of covalent bond between aluminum, carbon, silicon, and hydrogen atoms. In fact, the adsorption of H_2 molecules can introduce spin polarization on the X–B_4N_{10}_NC which specifies that these surfaces may be employed as magnetic adsorbent surface. Regarding IR spectroscopy, doped nanocells of H_2@Si–B_4N_{10}_NC ≈ H_2@Al–B_4N_{10}_NC > H_2@C–B_4N_{10}_NC, respectively, have the most fluctuations and the highest adsorption tendency for hydrogen molecules which can address specific questions on the individual effect of charge carriers (hydrogen molecule-nanocell), as well as doping atoms on the overall structure. Based on the results of ΔG_R° amounts in this research, the maximum efficiency of Al, C, Si atoms doping of B_5N_{10}_NC for H_2 molecules adsorption depends on the covalent bond between hydrogen atoms and X–B_4N_{10}_NC as a potent sensor for hydrogen storage. Finally, high selectivity of atom-doped on boron nitride nanocell for H_2 molecules adsorption has been resulted as: H_2@Si–B_4N_{10}_NC > H_2@Al–B_4N_{10}_NC ≫ H_2@C–B_4N_{10}_NC. Our findings prepare important visions into the potential of employing X (X = Al, C, Si)–B_4N_{10} nanocells in hydrogen-based energy-storage approaches. The results denote that H_2@X–B_4N_{10}_NC are stable compounds, with the most stable adsorption site being the center of the cage ring.

Keywords: BN-nanocell, energy storage, hydrogen adsorption, atom doping, materials modelling

DOI: 10.1134/S1990793124700131

INTRODUCTION

The aim of the present work is to apply TM doped on the B_5N_{10} nanocell clusters and to investigate the structure by theoretical calculation. To understand the atomic structure models and structural stabilities of the clusters, total energy calculations were carried out. The present study will give us a guideline for designing the BN clusters, which are expected as the future nanoscale devices. Boron nitride nanomaterials have been used owing to their unparalleled specifications of eco-friendly attributes for pollutant adsorption and semiconducting property [1–4].

Boron nitride nanometerials usually exhibits semi-leading behavior, which is considered a proper alternative to carbon nanotubes. The properties of boron and nitrogen atoms which are the first neighbors of carbon in the periodic table, make boron nitride as an interesting subject of numerous studies [5–7].

In recent years, different investigations on the adsorption of chemical contaminants and applying

various boron nitride nanostructures as adsorbents for water purification have been studied [8–10].

Various physical shapes of boron nitride (BN)-based nano adsorbents such as nanoparticles, fullerenes, nanotubes, nanofibers, nanoribbons, nanosheets, nanomeshes, nanoflowers, and hollow spheres have been broadly considered possible adsorbents owing to their exceptional characteristics such as large surface area, structural variability, great chemical/mechanical strength, abundant structural defects, high reactive sites, and functional groups [11, 12].

H_2 gas is mostly preserved either by liquefaction under high compressing pressure [13–16] or by adsorption on the surface or interstitial region of material cavity [17–19]. In relation to this, the adsorption of H_2 on the surface of 2D materials has advantages in terms of safe functionality and cost-effectiveness. For the effective utilization of H_2 in fuel cells, the adsorption energy and gravimetric weight percentage on the adsorbent should be sufficiently high [20–24].

The adsorption-desorption kinetics and the strength of binding energy ought to be intermediate for hydrogen to bind on the material surfaces with an optimal adsorption energy range. Owing to the obvious reasons mentioned above, we have explored the possibility of using boron nitride nanocells doped with aluminum, carbon, and silicon for H_2 storage by employing first-principles calculations. We have analyzed the structural and electronic properties of X (Al, C, Si)–B_4N_{10} nanocells using state-of-the-art computational techniques.

Adsorption involving charged adsorbates causes a change in the double layer and the potential at the outer Helmholtz plane, influencing the adsorption rates of both anodic and cathodic reactions. The first three modes are intimately with adsorption and the double layer involves interaction of the adsorbates and the intermediate products. These compounds have been formed during the partial electrochemical reactions and interaction of the adsorbed intermediates with organic molecules which can either inhibit or enhance electrode reaction rate [25–31].

The energy of interaction of a molecule close to a solid surface can be designed as a few terms for the molecule interacting with unit cells for a periodic lattice. Similar theories and approaches can be applied to explain the interaction of two molecules at the surface, or the interaction of the surface with islands or layers of adsorbed molecules [32–39]. A continuum model can be used to describe interactions of a molecule with a surface electric dipole layer formed by the rearrangement of atomic positions and electronic charge at the surface [40–47].

Particularly, this research work aims to assess the influences of doping atoms of Al, C, Si on the X–B_4N_{10}_NC for increasing hydrogen detection through measurement of some parameters containing charge transfer, electric potential, electromagnetic and thermodynamic properties, surface area, functional group and examine the ability of applying (Al, C, Si)–B_4N_{10} nanocells in hydrogen-based energy-storage approaches.

In this article, the data has evaluated the efficiency of boron nitride nanocell doped with aluminum, carbon, silicon (X–B_4N_{10}_NC) for hydrogen detection. In fact, it can be remarked the chemisorptive nature of the bond among the hydrogen molecules with boron and nitrogen elements through the equilibrium distribution of doping atoms, B_5N_{10}_NC, and a monolayer attribute.

THEORY, COMPUTATIONAL METHOD, AND MATERIALS

Adsorption of Hydrogen Molecules on X–B_4N_{10}_NC

Boron nitride (BN) nanocell clusters of B_5N_{10} were optimized with a bond length of about 1.7 Å. The atoms of Aluminum, Carbon and Silicon have been doped on the top of the B_5N_{10} through substituting with boron atom. The aim of this study is to adsorb hydrogen molecules in the energy storage cell [48, 49] as an eco-friendly approach by using (Al, C, Si)-doped B_5N_{10}_NC (Fig. 1).

The structures of the adsorbent (X–B_4N_{10}_NC) and the adsorbate (H_2 molecules) were built using GaussView 6.1 [37]. Then, for all complexes, the adsorption energies were obtained through the following equation: $E_{ads} = E_{complex} - (E_{nanocage} + E_{gas})$.

Figure 1 has shown the process adsorption of H_2 molecules on the X–B_4N_{10}_NC surface which towards formation of complexes containing H–H@Al–B_4N_{10}_NC, H–H@C–B_4N_{10}_NC, and H–H@Si–B_4N_{10}_NC complexes by molecular modeling computations.

The charge distribution of mentioned complexes is calculated due to the Bader charge analysis [50]. The trapping of H_2 molecules by X–B_4N_{10}_NC (X=Al, C, Si) were successfully incorporated due to binding formation consisting of H → Al, H → C, H → Si (Fig. 1). An extensive study of adsorption and diffusion of hydrogen atoms on B_4N_{10}_NC surface doped with Al, C and Si was performed by means of computational methods.

Density Functional Theory

Progress of the applied density functional theory (DFT) technique became remarkable after W. Kohn and L. J. Sham presented their equations as Kohn–Sham equations [51–58]. Regarding DFT method [59–64], the behavioral mechanism of Al, C, Si addition to promote hydrogen adsorption on the surface of B_5N_{10}_NC is investigated based on the adsorption energy, charge transfer and density of states. The investigated results indicate that H bonding with a doped atom of Al or C or Si on the B_5N_{10}_NC surface

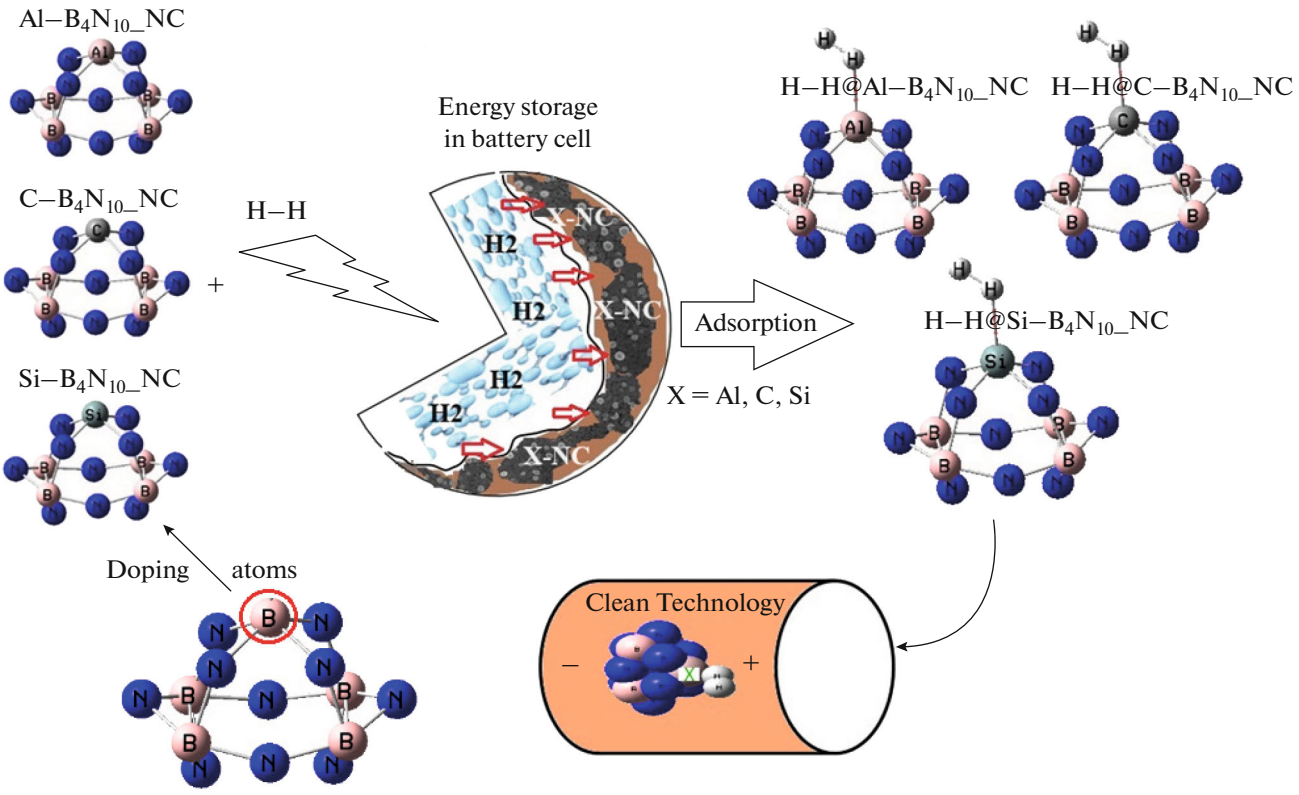

Fig. 1. Application of pristine B_5N_{10}_NC and doped complexes of Al–B_4N_{10}_NC, C–B_4N_{10}_NC, and Si–B_4N_{10}_NC, respectively, for adsorption of hydrogen molecules in the energy storage cell towards formation of complexes: (a) H_2@B_5N_{10}_NC (b) H_2@Al–B_4N_{10}_NC, (c) H_2@C–B_4N_{10}_NC, and (d) H_2@Si–B_4N_{10}_NC, complexes using CAM–B3LYP–D3/6-311 + G(*d*, *p*), LANL2DZ calculation. (Note: the sign of adsorption is shown with @).

could promote the H_2 molecule to dissociate into two H atoms that bond with the doped Al or C or Si atom on the B_5N_{10}_NC surface.

The newly formed H–Al, H–C or H–Si bond constitutes the channel of electron transfer between hydrogen atom and Al or C or Si and weaken the adjacent H–H bonding effect, which are conducive to the formation of new H–Al, H–C or H–Si bonds. Applying Gaussian 16 revision C.01 program [65] and GaussView 6.1 [66], the function of exchange through B3LYP level of theory and the phrase of density approximation in mechanic quantum [62–64] have been accomplished. This research article wants to provide important viewpoints of hydrogen adsorption on the boron nitride surface and DFT calculations were run with the goal of understanding microscopic adsorption amount of the hydrogen atom on the surface of B_5N_{10}_NC doped with of Al, C, or Si.

Nuclear Quadrupole Resonance and Nuclear Magnetic Resonance

The methodology of nuclear quadrupole resonance spectroscopy (NQR) is a technology for analyzing chemical compounds. NQR transitions of nuclei are capable of being found in the lack of a magnetic field. The NQR resonance is mediated by the interaction of the electric field gradient (EFG) with the quadrupole moment of the nuclear charge distribution [67, 68]. As the EFG at the spot of a nucleus in a certain material is assigned by the valence electrons deal with the special bond with other close nuclei, the NQR frequency at which transitions occur is unique for a mentioned material. A special NQR frequency in a material is symmetrical to the outcome of the nuclear quadrupole moment, an attribute of the nucleus, and the EFG in the vicinity of the nucleus [69, 70].

The nuclear magnetic resonance (NMR) supplies an exact perspective of adsorbed hydrogen molecule that offers immediate feedback for optimizing the process status. NMR through chemical shielding tensors present the Information about defect structures, pore surfaces, atom doped cages during hydrogen adsorption process [71]. The NMR data of isotropic (σ_{iso}) and anisotropic (σ_{aniso}) shielding tensors of hydrogen molecules trapped in the X–B_4N_{10}_NC towards formation of H_2@X–B_4N_{10}_NC complexes have been

computed by Gaussian 16 revision C.01 program package [65].

RESULTS AND DISCUSSION

Projected Density of State

The projected density of state (PDOS) of H_2@ B_5N_{10}_NC and H_2@(Al, C, Si)–B_4N_{10}_NC through hydrogen molecules adsorption (Fig. 2). The appearance of the energy states (*p*-orbital) of Al, C, Si, N within the gap of (Al, C, Si)–B_4N_{10}_NC induces the reactivity of the system. It is clear from the figure that after trapping with hydrogen molecules, there is a significant contribution of *p*-orbital in the unoccupied level. Therefore, the curve of partial PDOS has described that the *s* states of H atoms and B in pristine B_5N_{10}_NC and Al, C, Si atoms in X–B_4N_{10}_NC overcome due to the conduction band (Fig. 2). A distinguished adsorption trait might be seen in H_2@X–B_4N_{10}_NC because of the potent interaction between the *s* states of hydrogen atoms with *p* states of Al, C, Si in X–B_4N_{10}_NC complexes.

H_2@B_5N_{10}_NC, H_2@Al–B_4N_{10}_NC, H_2@C–B_4N_{10}_NC, and H_2@Si–B_4N_{10}_NC complexes through hydrogen adsorption, respectively, have the most contribution at the middle of the conduction band between –5 to –10 eV, while contribution of boron and nitrogen states are enlarged and similar together, and adsorbing of H_2 depicts interfacial electronic of the B_4N_{10}_NC for selection of hydrogen molecules. Figure 2a shows the capture of hydrogen molecules by pristine B_4N_{10}_NC. Then, H_2@Al–B_4N_{10}_NC has indicated sharp peaks for Al atom close to H atoms in Fig. 2b. H_2@C–B_4N_{10}_NC (Fig. 2c) has exhibited strong peaks for C atom close to H atoms. Furthermore, the sharp Si graph near H atoms in H_2@ Si–B_4N_{10}_NC (Fig. 2d) has been indicated. Therefore, the order ability of hydrogen adsorption by doping atoms of Al, C, Si on X–B_4N_{10}_NC based on the PDOS might be shifted as: Si–B_4N_{10}_NC > C–B_4N_{10}_NC > Al–B_4N_{10}_NC.

Nuclear Quadrupole Resonance Analysis

As the EFG at the citation of the nucleus in H_2 is allocated by the valence electrons twisted in the attachment with close nuclei of X–B_4N_{10}_NC (X = Al, C, Si) through trapping of hydrogen molecules, the NQR frequency at which transitions occur is particular for H_2@(Al, C, Si)–B_4N_{10}_NC complexes (Fig. 3). In fact, gas molecules of H_2 can be adsorbed on the top of the pristine B_5N_{10}_NC (Fig. 3a) through B(13) which has been replaced with Al(13) (Fig. 3b), C(13) (Fig. 3c), or Si(13) (Fig. 3d) due to doping technique.

In this research work, the electric potential as the quantity of work energy through carrying over the electric charge from one position to another position in the essence of electric field has been evaluated for H_2@B_5N_{10}_NC, H_2@Al(13)–B_4N_{10}_NC, H_2@C(13)–B_4N_{10}_NC, and H_2@Si(13)–B_4N_{10}_NC complexes (Table 1 and Fig. 3).

In Table 1, the Bader charge and electronic potential properties of B(13) in B_5N_{10}_NC and Al(13), C(13), Si(13) in X–B_4N_{10}_NC through adsorption of hydrogen molecules on atom–doped boron nitride nanocell have been investigated. The amounts indicate that with increasing the negative charge of different atoms, the electric potential resulted from NQR calculations increase. Moreover, the doping atoms of Al(13), C(13), Si(13) on the B_4N_{10}_NC have shown the most potential for accepting the electron from electron donor of H(16) and H(17) in H_2 adsorbed on the B_4N_{10}_NC (Table 1).

Furthermore, in Fig. 4, it has been sketched the electric potential of nuclear quadrupole resonance for some atoms of Al, C, Si/B, N in X–B_4N_{10}_NC and H atoms of H_2 molecule trapped on atom–doped boron nitride nanocell which has been calculated by CAM–B3LYP–D3/EPR–3, LANL2DZ.

In Fig. 4a, it was observed the behavior of H_2 adsorption on the pristine B_5N_{10}_NC with high sensitivity based on relation coefficient of R^2 = 0.9947, Al(13)–B_4N_{10}_NC with high fluctuation and R^2 = 0.9276 (Fig. 4b). Adsorption of H_2 on the C(13)–B_4N_{10}_NC in Fig. 4c has illustrated the higher sensing than Al(13)–B_4N_{10}_NC with $R^2 = 0.9769$. In addition, Fig. 4d has resulted that Si–B_4N_{10}_NC has a good detecting for H_2 adsorption in the battery cell based on the relation coefficient of $R^2 = 0.9689$.

It's vivid that the curve of pristine B_5N_{10}_NC is waved through doping of some atoms for capturing the H_2 molecules. The fluctuated peaks for electric potential have been shown around H_2 trapping on the X–B_4N_{10}_NC which demonstrates the electron accepting specifications of hydrogen versus the aluminum, carbon and silicon doped on the B_5N_{10}_NC (Figs. 4b, 4c, 4d). Besides, it can be considered that carbon (Fig. 4c) and silicon (Fig. 4d) as the semiconductor elements in the functionalized B_4N_{10}_NC might have more impressive sensitivity for accepting the electrons from H atoms in the process of adsorption mechanism. Electric potential and capacitance have a breadth of applications within power generation and energy storage. Properly understanding the electric potential in a sys-

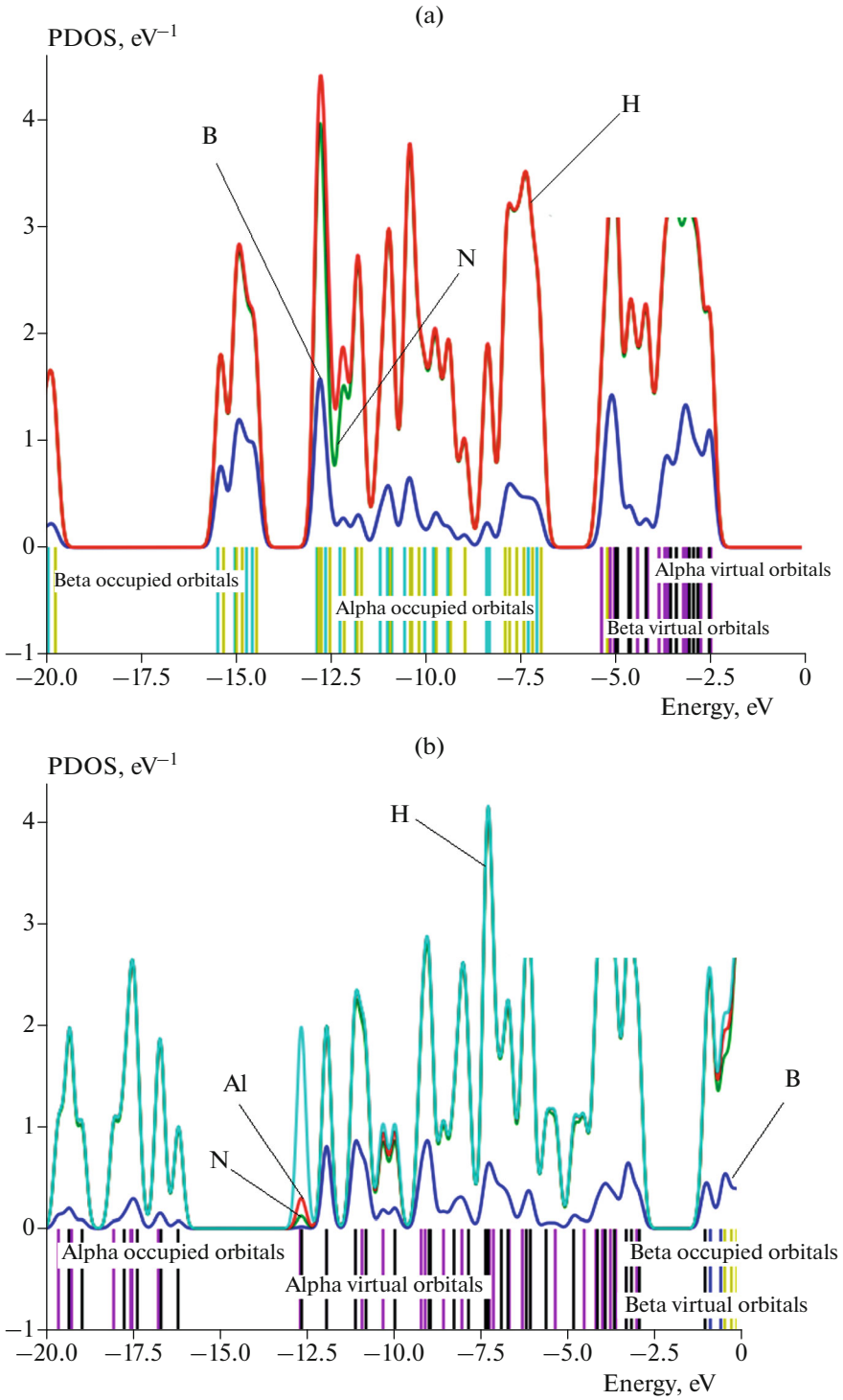

Fig. 2. The projected density of state of H_2 adsorbed on pristine and X(X = Al, C, Si)-doped B_5N_{10}_NC including (a) H_2@B_5N_{10}_NC, (b) H_2@Al–B_4N_{10}_NC, (c) H_2@C–B_4N_{10}_NC, and (d) H_2@Si–B_4N_{10}_NC complexes by CAM–B3LYP–D3/6–311+G(*d*, *p*), LANL2DZ.

tem can create materials in novel ways. However, aluminum-doped on B_5N_{10}_NC (adsorbent) has shown the lowest fluctuation (R^2 = 0.9276) between Bader charge versus electric potential extracted from NQR parameters and the lowest negative atomic charge including 1.1541 coulomb in H_2@Al–B_4N_{10}_NC which can be an appropriate option for H_2 molecules (adsorbate) after C–B_4N_{10}_NC with 0.1167 coulomb

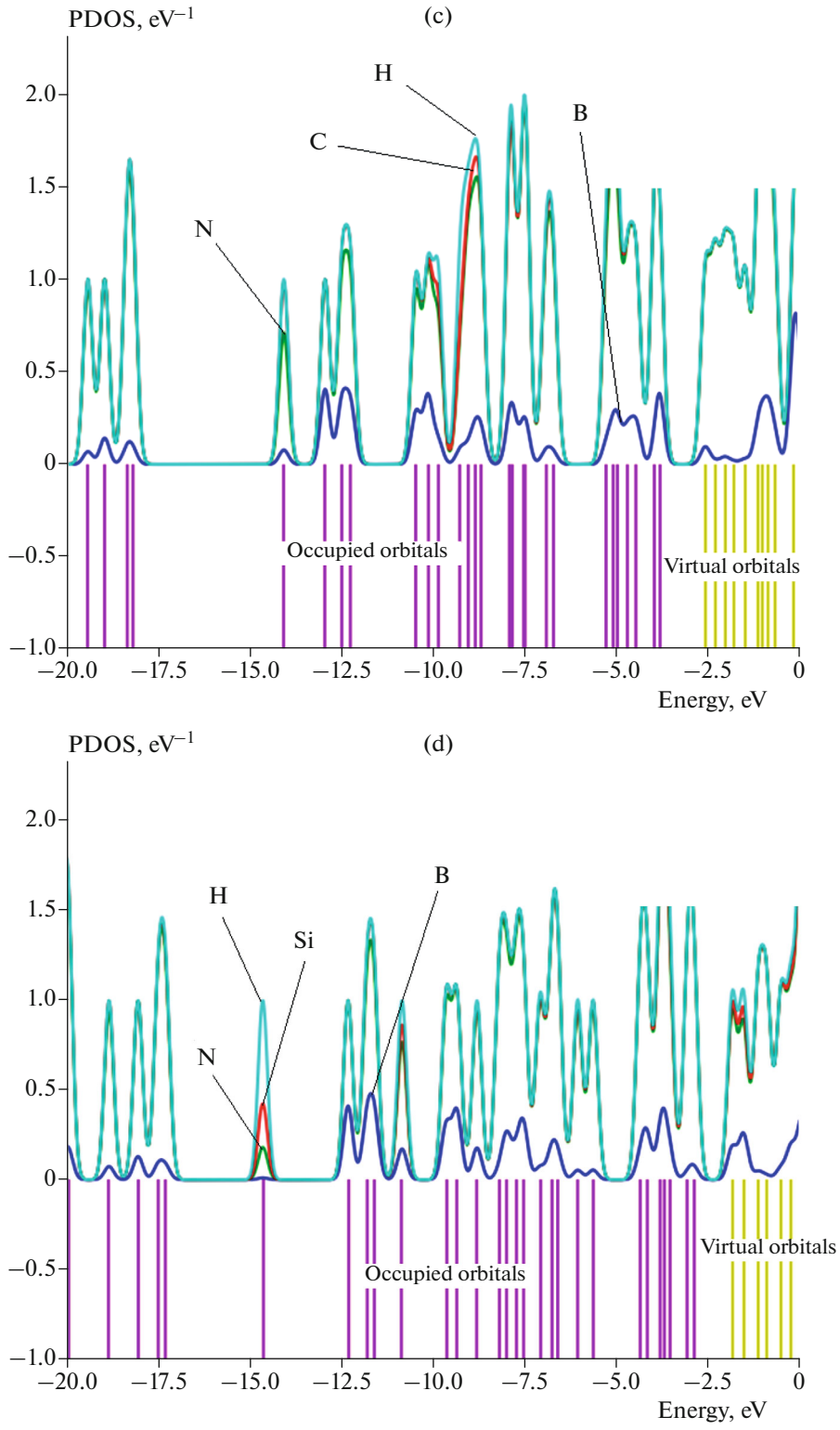

Fig. 2. (Contd.)

on C atom and Si $-B_4N_{10}$_NC with 1.0620 coulomb on Si atom, the highest tendency for electron accepting in the adsorption current (Table 1).

In fact, the uptake of H_2 molecules has been known to be associated with X–B_4N_{10}_NC, indicating that the adsorbed hydrogen molecules in the X–doped

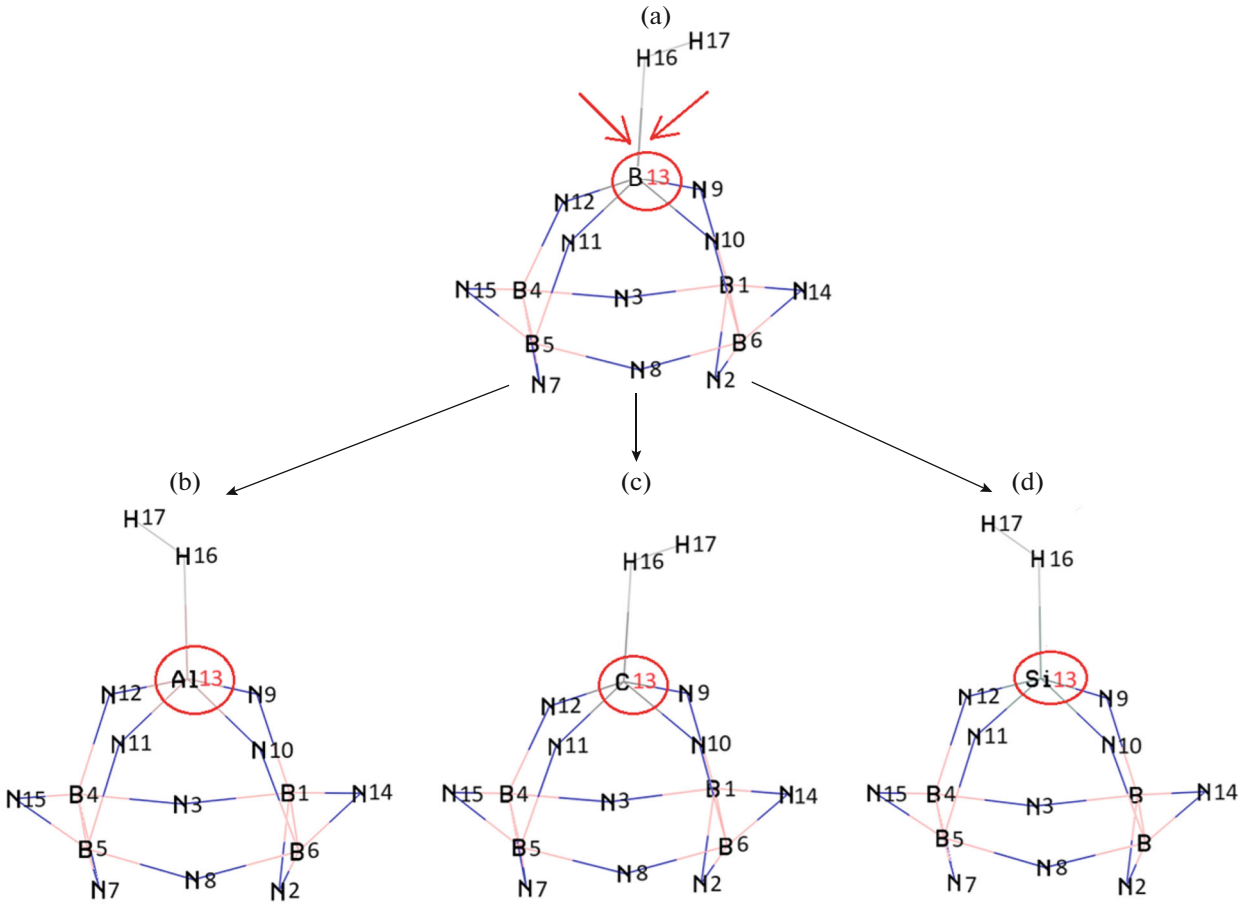

Fig. 3. Optimized structures of H_2 adsorption on the surface of (a) pristine B_5N_{10}_NC and X–B_4N_{10}_NC (X = Al, C, Si) toward forming of (b) H_2@Al(13)–B_4N_{10}_NC, (c) H_2@C(13)–B_4N_{10}_NC and (d) H_2@Si(13)–B_4N_{10}_NC.

nanocell can be internalized through a different pathway from pristine nanocell.

Analysis of Nuclear Magnetic Resonance Spectra

Nuclear magnetic resonance spectra of X (X = Al, C, Si)–B_4N_{10}_NC complexes as the potent sensor for adsorbing H_2 molecules can unravel the efficiency of X–B_4N_{10}_NC for saving clean energy as an ecofriendly approach in battery cells. The NMR data of isotropic (σ_{iso}) and anisotropic shielding tensors (σ_{aniso}) of hydrogen molecules trapped in the pristine B_5N_{10}_NC and X (X = Al,C,Si)–B_4N_{10}_NC towards formation of H_2@B_5N_{10}_NC, H_2@Al(13)–B_4N_{10}_NC, H_2@C(13)–B_4N_{10}_NC, and H_2@Si(13)–B_4N_{10}_NC complexes, respectively, (Fig. 3) have been reported in Table 2.

In Table 2, NMR data has reported the notable amounts for H_2 molecules which were adsorbed on the pristine B_5N_{10}_NC and X (X = Al, C, Si)–B_4N_{10}_NC as the selective sensor for saving energy. The observed increase in the chemical shift anisotropy spans for H atoms adsorption on the pristine B_5N_{10}_NC are around N(7), N(8), N(9), N(10), N(11), N(12), N(14), N(15) and also for X–B_4N_{10}_NC are near N(9), N(10), N(11), N(12), N(14) and N(15). The observed weak signal intensity near the parallel edge of the nanocell pattern may be due to boron binding induced non-spherical distribution of these complexes.

It is remarkable that doping of Al(13), C(13), Si(13) on B_5N_{10}_NC might promote the stability of nanocell that results in enhanced magnetic alignment of complexes. Interestingly, the reported results show that Al(13), C(13), Si(13) elements can be optimized to achieve optimal alignment of nanocell in the presence of an applied magnetic field. In fact, the adsorption of H_2 can introduce spin polarization on the X–B_4N_{10}_NC which indicates that these surfaces might be applied as magnetic scavenging surface as the hydrogen detector. Isotropic and anisotropic shielding fluctuate with the occupancy in the electron accepting hydrogen molecules trapped in the atom-doped on the boron nitride nanocell.

Figure 5 exhibited a considerable deviation from B_5N_{10}_NC after doping atoms of Al(13), C(13) and

Table 1. The electric potential (E_p/a.u.) and Bader charge (Q/coulomb) through NQR calculation for H_2@B_5N_{10}_NC, H_2@Al(13)–B_4N_{10}_NC, H_2@C(13)–B_4N_{10}_NC, and H_2@Si(13)–B_4N_{10}_NC complexes using CAM–B3LYP–D3/EPR–3, LANL2DZ calculation

H_2@B_5N_{10}_NC			H_2@Al–B_4N_{10}_NC			H_2@C–B_4N_{10}_NC			H_2@Si–B_4N_{10}_NC		
atom	Q	E_p	atom	Q	E_p	atom	Q	E_p	atom	Q	E_p
B(1)	0.2814	−11.2438	B(1)	0.2839	−11.3117	B(1)	0.2931	−11.2693	B(1)	0.3270	−11.2771
N(2)	−0.1366	−18.302	N(2)	−0.1792	−18.1494	N(2)	−0.1510	−18.0901	N(2)	−0.1660	−18.1268
N(3)	−0.1180	−18.3034	N(3)	−0.1159	−18.1259	N(3)	−0.1379	−18.0761	N(3)	−0.1618	−18.1185
B(4)	0.2588	−11.2466	B(4)	0.2876	−11.312	B(4)	0.2948	−11.2666	B(4)	0.3184	−11.2819
B(5)	0.2807	−11.2455	B(5)	0.3006	−11.3062	B(5)	0.2904	−11.2772	B(5)	0.3185	−11.2810
B(6)	0.2752	−11.2442	B(6)	0.3117	−11.2944	B(6)	0.2924	−11.2764	B(6)	0.3300	−11.2784
N(7)	−0.1376	−18.3078	N(7)	−0.1707	−18.1464	N(7)	−0.1528	−18.0921	N(7)	−0.1615	−18.1283
N(8)	−0.1379	−18.3025	N(8)	−0.1542	−18.1437	N(8)	−0.1350	−18.0832	N(8)	−0.1527	−18.1068
N(9)	−0.1623	−18.3101	N(9)	−0.3639	−18.2117	N(9)	−0.1062	−18.0879	N(9)	−0.3435	−18.1860
N(10)	−0.1742	−18.3121	N(10)	−0.3709	−18.2134	N(10)	−0.1072	−18.0907	N(10)	−0.3518	−18.1849
N(11)	−0.1477	−18.2944	N(11)	−0.3338	−18.1898	N(11)	−0.0962	−18.0852	N(11)	−0.3312	−18.1767
N(12)	−0.1642	−18.2995	N(12)	−0.3666	−18.1923	N(12)	−0.1076	−18.0697	N(12)	−0.3391	−18.1699
B (13)	0.2247	−11.2175	**Al (13)**	1.1541	−43.6855	**C (13)**	0.1167	−14.5183	**Si (13)**	1.0620	−48.3278
N(14)	−0.1300	−18.285	N(14)	−0.1615	−18.1255	N(14)	−0.1466	−18.0835	N(14)	−0.1892	−18.1337
N(15)	−0.1482	−18.2932	N(15)	−0.1751	−18.1393	N(15)	−0.1410	−18.0794	N(15)	−0.1797	−18.1293
H(16)	0.0170	−0.99642	H(16)	−0.0373	−1.0583	H(16)	0.0199	−1.16911	H(16)	−0.0226	−1.0145
H(17)	0.1190	−0.96945	H(17)	0.0913	−1.0270	H(17)	−0.0256	−1.20803	H(17)	0.0444	−1.1055

Si(13) on the nanocell through interaction with H(16) of H_2 molecules. Adsorption of H_2 molecules on the pristine B_5N_{10}_NC (Fig. 5a), and complexes of Al(13)–B_4N_{10}_NC (Fig. 5b), C(13)–B_4N_{10}_NC (Fig. 5c), and Si(13)–B_4N_{10}_NC (Fig. 5d) denote the fluctuation in the chemical shielding during ion trapping. Figures 5b, 5c, 5d shows the gap chemical shielding between aluminum, carbon, silicon doping of X–B_4N_{10}_NC complexes and hydrogen molecules. The yield of electron accepting for doping atoms on the X–B_4N_{10}_NC complexes through hydrogen molecules adsorption can be ordered as: Al > Si ⩾ C that approves the possibility of covalent bond between aluminum, carbon, silicon, and hydrogen atoms in H_2 molecules towards energy storage in battery technology.

In the NMR spectroscopy, it has been observed the remarkable peaks around interaction of H_2 molecules through adsorbing on the X–B_4N_{10}_NC during molecule detection; however, there are some fluctuations in the chemical shielding behaviors of isotropic and anisotropy attributes. Therefore, the authors believe that the extracted results would be useful in the design of X–B_4N_{10}_NC based doped nanomaterials for increasing the adsorption of hydrogen molecules in addition to the structural studies using solid-state and solution NMR technique.

Thermodynamic Parameters Extracted from Infrared Spectra

The infrared (IR) computations have been attained for adsorption of H_2 molecules by pristine B_5N_{10}_NC and X–B_4N_{10}_NC during hydrogen sensing. Therefore, it has been simulated the several clusters containing H_2@ B_5N_{10}_NC (Fig. 6a), H_2@ Al–B_4N_{10}_NC (Fig. 6b), H_2@ C–B_4N_{10}_NC (Fig. 6c), and H_2@ Si–B_4N_{10}_NC (Fig. 6d) using CAM–B3LYP–D3/6-311+G (*d*, *p*), LANL2DZ.

The pristine B_5N_{10}_NC has shown the graph in the frequency range between 200–1800 cm^{-1} for H_2@ B_5N_{10}_NC with a sharp peak around 1667.11 cm^{-1} (Fig. 6a). Thus, our investigation can provide benchmark theoretical results to find the experimental IR phonon modes of homogeneous boron nitride nanocages.

The graph of Fig. 6b has been observed in the frequency range between 100–2000 cm^{-1} for H_2@Al–B_4N_{10}_NC with several sharp peaks around 177.92, 483.81, 910.24, and 1645.95 cm^{-1}. Figure 6c has shown the frequency range between 200–2000 cm^{-1} for H_2@C–B_4N_{10}_NC with a sharp peak around 1729.19 cm^{-1}. Fig. 6d has indicated the fluctuation of frequency between 1000–2500 cm^{-1} for H_2@Si–B_4N_{10}_NC with a sharp peak around 1531.05 cm^{-1}.

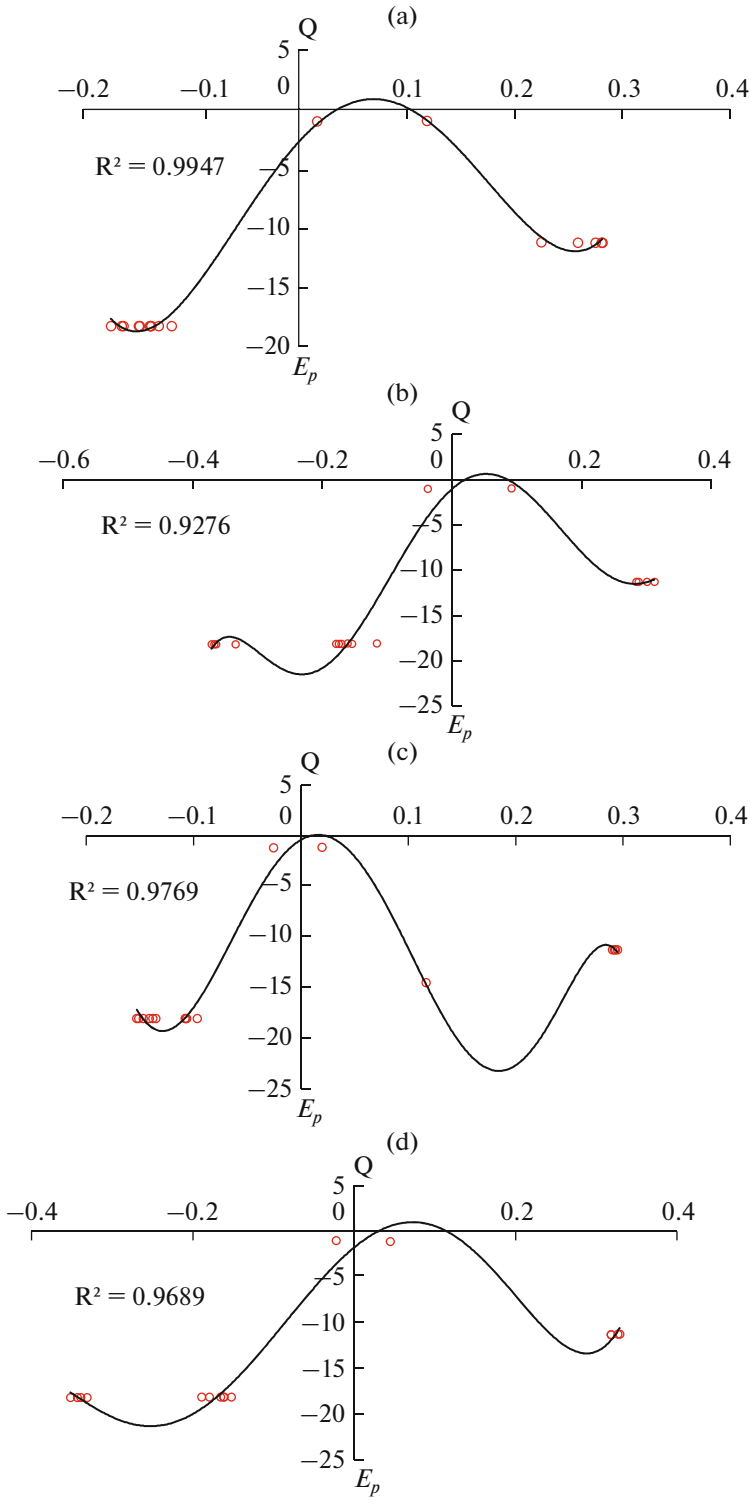

Fig. 4. Electric potential (a.u.) versus Bader charge (coulomb) through NQR calculation for (a) H–H@B_5N_{10}_NC, (b) H–H@Al(13)–B_4N_{10}_NC, (c) H–H@C(13)–B_4N_{10}_NC, (d) H–H@Si(13)–B_4N_{10}_NC complexes by CAM–B3LYP–D3/EPR–3, LANL2DZ.

The IR spectra of H_2 adsorption with X–B_4N_{10}_NC has demonstrated that the structure of the dominant complex correlates with the electron potency of doped X (Al, C, Si) on the B_5N_{10}_NC. The doped nanocell of Al–B_4N_{10}_NC (Fig. 6b) has shown the most fluctuations and the highest tendency for

Table 2. Data of NMR shielding tensors for selected atoms of $H_2@B_5N_{10}$_NC, $H_2@Al(13)-B_4N_{10}$_NC, $H_2@C(13)-B_4N_{10}$_NC and $H_2@Si(13)-B_4N_{10}$_NC complexes using CAM–B3LYP–D3/6-311+G(*d*, *p*), LANL2DZ calculation

$H_2@B_5N_{10}$_NC			$H_2@Al-B_4N_{10}$_NC			$H_2@C-B_4N_{10}$_NC			$H_2@Si-B_4N_{10}$_NC		
Atom	σ_{iso}	σ_{aniso}	atom	σ_{iso}	σ_{aniso}	atom	σ_{iso}	σ_{aniso}	atom	σ_{iso}	σ_{aniso}
B(1)	74.0140	73.6296	B(1)	97.5342	83.4065	B(1)	104.4465	91.6792	B(1)	75.3800	57.4893
N(2)	686.3846	645.9651	N(2)	256.1209	636.6725	N(2)	122.3461	619.5041	N(2)	33.5650	576.4161
N(3)	229.0012	250.5861	N(3)	62.4289	79.1904	N(3)	1555.4302	2736.9396	N(3)	1098.1924	2362.5034
B(4)	88.0316	75.4231	B(4)	105.7341	72.8788	B(4)	100.0820	126.1374	B(4)	104.4862	42.5119
B(5)	65.8065	90.7506	B(5)	95.4999	55.8852	B(5)	126.1374	40.3731	B(5)	60.9480	54.5121
B(6)	75.1814	73.5828	B(6)	78.0999	73.1263	B(6)	110.9670	62.8131	B(6)	56.0680	69.7371
N(7)	639.8711	485.0100	N(7)	173.5651	565.3693	N(7)	248.3122	382.1473	N(7)	49.5610	1405.1233
N(8)	728.8636	908.0240	N(8)	78.6518	254.4183	N(8)	516.6918	1188.9826	N(8)	1110.1238	1984.6541
N(9)	723.6043	689.0534	N(9)	472.6234	831.2210	N(9)	593.2418	1206.1623	N(9)	18.2632	5065.2153
N(10)	759.0698	812.3451	N(10)	569.4159	703.5432	N(10)	871.5872	1747.4894	N(10)	528.9146	2567.9010
N(11)	596.0904	902.9599	N(11)	508.1483	940.5764	N(11)	1075.3603	1808.5469	N(11)	446.9468	4452.6584
N(12)	588.3767	925.3864	N(12)	275.1350	706.0008	N(12)	601.1167	1086.0253	N(12)	146.3612	1615.6490
B(13)	80.3281	95.8087	**Al (13)**	522.1327	157.5390	**C (13)**	106.4980	79.7876	**Si (13)**	722.9049	178.4777
N(14)	319.3553	1073.7091	N(14)	26.4101	596.7615	N(14)	0.5312	1401.6259	N(14)	253.7520	706.9400
N(15)	295.0201	1045.0049	N(15)	18.6650	593.7138	N(15)	268.2439	1157.8911	N(15)	46.2129	1894.7646
H(16)	23.9160	2.8335	H(16)	23.4528	2.7576	H(16)	24.2942	6.7582	H(16)	16.5391	32.8420
H(17)	21.5253	1.8654	H(17)	21.2929	2.8108	H(17)	26.5494	3.3605	H(17)	22.6766	25.8481

Table 3. The thermodynamic characters of $H_2@B_5N_{10}$_NC, $H_2@Al-B_4N_{10}$_NC, $H_2@C-B_4N_{10}$_NC, and $H_2@Si-B_4N_{10}$_NC complexes using CAM–B3LYP–D3/6-311+G (d,p), LANL2DZ calculation

Compound	$\Delta E^{\circ}_{ads} \times 10^{-3}$, kcal/mol	$\Delta H^{\circ}_{ads} \times 10^{-3}$, kcal/mol	$\Delta G^{\circ}_{ads} \times 10^{-3}$, kcal/mol	S°_{ads}, cal/K mol	Dipole moment, Debye
B_5N_{10}_NC	–420.550	–420.549	–420.579	100.650	0.2020
$Al-B_4N_{10}$_NC	–406.553	–406.553	–406.584	105.620	3.9464
$C-B_4N_{10}$_NC	–428.953	–428.952	–428.982	99.184	1.7591
$Si-B_4N_{10}$_NC	–407.701	–407.700	–407.730	102.387	1.2666
$H_2@B_5N_{10}$_NC	–421.456	–421.455	–421.488	108.874	1.7938
$H_2@Al-B_4N_{10}$_NC	–551.051	–551.050	–551.081	104.003	4.4034
$H_2@C-B_4N_{10}$_NC	–424.231	–424.231	–424.260	99.710	1.4722
$H_2@Si-B_4N_{10}$_NC	–580.207	–580.206	–580.235	95.419	2.8124

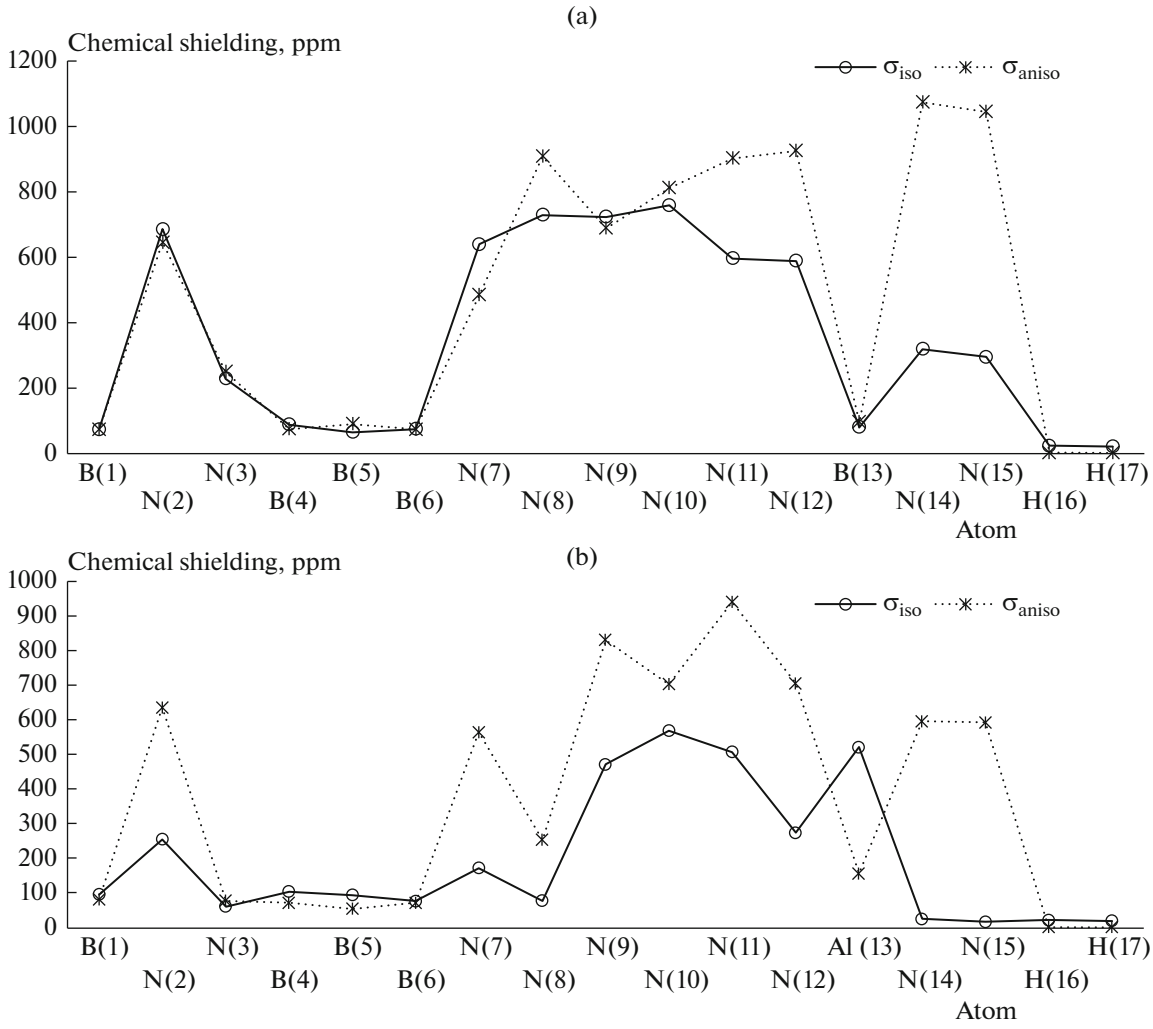

Fig. 5. The NMR spectra for (a) H_2@B_5N_{10}_NC, (b) H_2@Al (13)–B_4N_{10}_NC, (c) H_2@C (13)–B_4N_{10}_NC, and (d) H_2@Si (13)–B_4N_{10}_NC complexes using CAM–B3LYP–D3/6–311+G(*d*, *p*), LANL2DZ.

adsorption of H_2 molecules than C–B_4N_{10}_NC and Si–B_4N_{10}_NC complexes, respectively, (Figs. 6c and 6d). Therefore, it can be found that IR spectroscopy of H_2-adsorbed Al–B_4N_{10}_NC is now well-placed to address specific questions on the individual effect of charge carriers (hydrogen molecule- nanocell), as well as doping atoms on the overall structure.

Table 3 through the thermodynamic specifications concluded that X (X = Al, C, Si)–B_4N_{10}_NC due to adsorption of H_2 might be more efficient sensors for detecting and absorbing the hydrogen molecules towards the energy storage in battery cells and its implication for clean energy technology. The small size of X (X = Al, C, Si)–B_4N_{10}_NC and the large surface area make them proper sample for different applications. Moreover, the optical attributes are also important at that size, which further enhance the significance of these compounds in photocatalytic applications.

Thermodynamic parameters of H_2 molecules adsorption on the X–B_4N_{10}_NC complexes have been determined using DFT theoretical technique. It has been shown that for a given number of hydrogen donor sites in H_2 molecules, the stabilities of complexes owing to doping atoms of Al, C, Si can be considered as: H_2@Si–B_4N_{10}_NC > H_2@Al–B_4N_{10}_NC ≫ H_2@C–B_4N_{10}_NC complexes (Table 3). The changes of Gibbs free energy versus dipole moment in could detect the maximum efficiency of Al, C, Si atoms doping of B_4N_{10}_NC for H_2 molecules adsorption through ΔG_R° which depends on the covalent bond between H_2 molecules and X–B_4N_{10}_NC as a potent sensor for air pollution removal (Table 3). The adsorption process of H_2 molecules on the X–B_4N_{10}_NC is affirmed by the ΔG_R° quantities:

$$\Delta G_{\text{ads}}^\circ = \Delta G_{\text{H}_2@\text{X}-\text{B}_4\text{N}_{10\text{NC}}}^\circ - \left(\Delta G_{\text{H}_2}^\circ + \Delta G_{\text{X}-\text{B}_4\text{N}_{10\text{NC}}}^\circ\right),$$

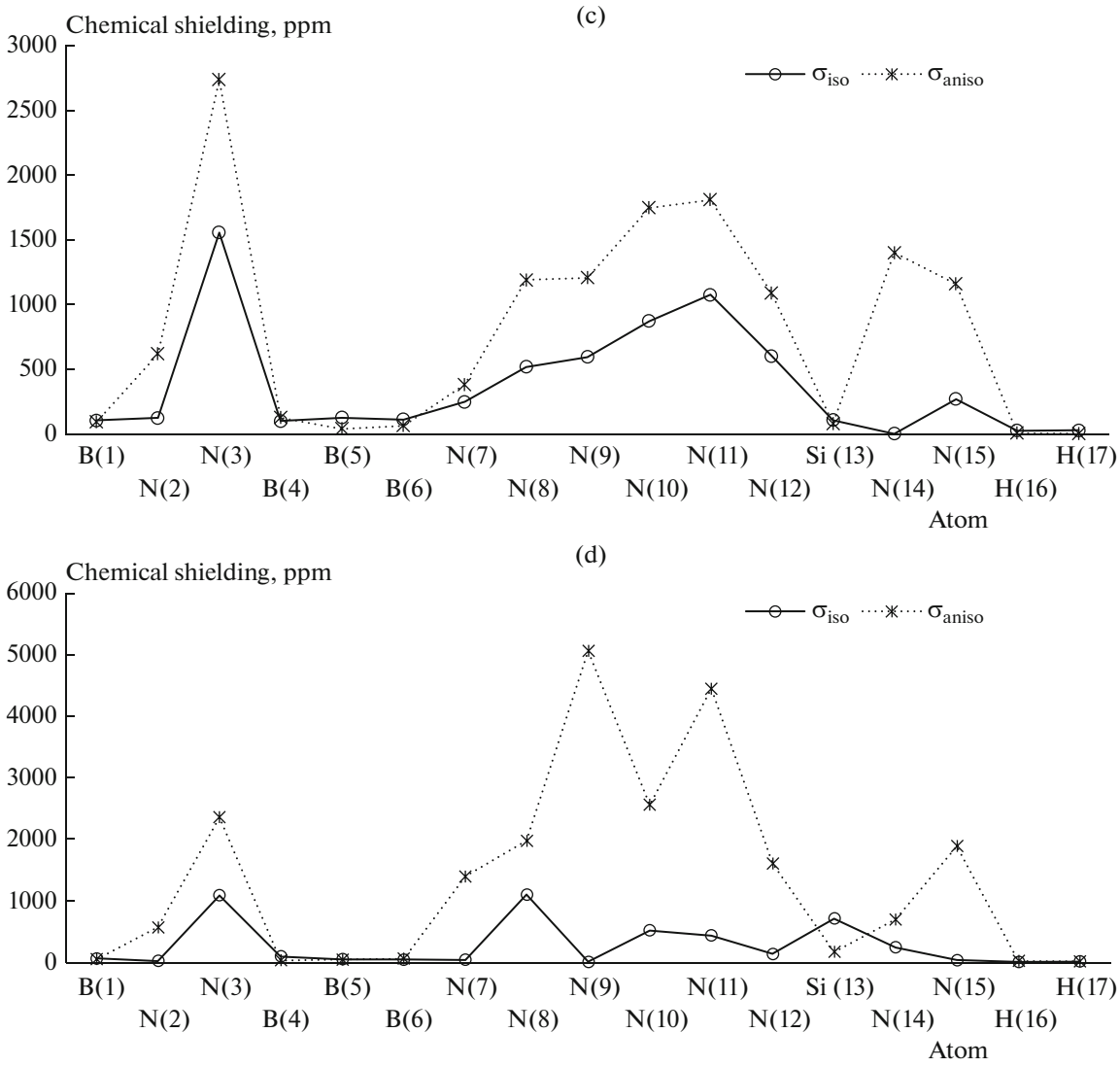

Fig. 5. (Contd.)

and

$$X = Al, C, Si.$$

Figure 6 has shown the key role of doped atoms containing Al, C, Si during interaction between the adsorbate of H_2 molecules as the electron donors and the adsorbent of Al–B_4N_{10}_NC, C–B_4N_{10}_NC, and Si–B_4N_{10}_NC complexes as electron acceptors. Therefore, the selectivity of atom-doped on boron nitride nanocell (hydrogen sensor) for H_2 adsorption can be resulted as: Si > Al ⩾ C (Table 3).

Many experimental discoveries have been gained on the related electrical characteristics, optical attributes, and thermal conductivities of boron nitride materials. Some experimental studies have given fundamental data support for achieving reversible hydrogen storage at room temperature [72]. Owing to the characteristics of nanoparticles, they are appropriate samples for different commercial and domestic applications, which contain catalysis, some energy storage research, and eco-friendly applications [73].

However, the consequences appear a gap remarking to the positive predictions and an inconsistence between each other. It denotes that the innovative boron nitride structures call for the progress of synthesis process. After that research accompanying practical basis with theoretical computations require to design the unique hydrogen storage mechanism, further supplying possible modification tactics to ameliorate their accomplishment in outcome [74].

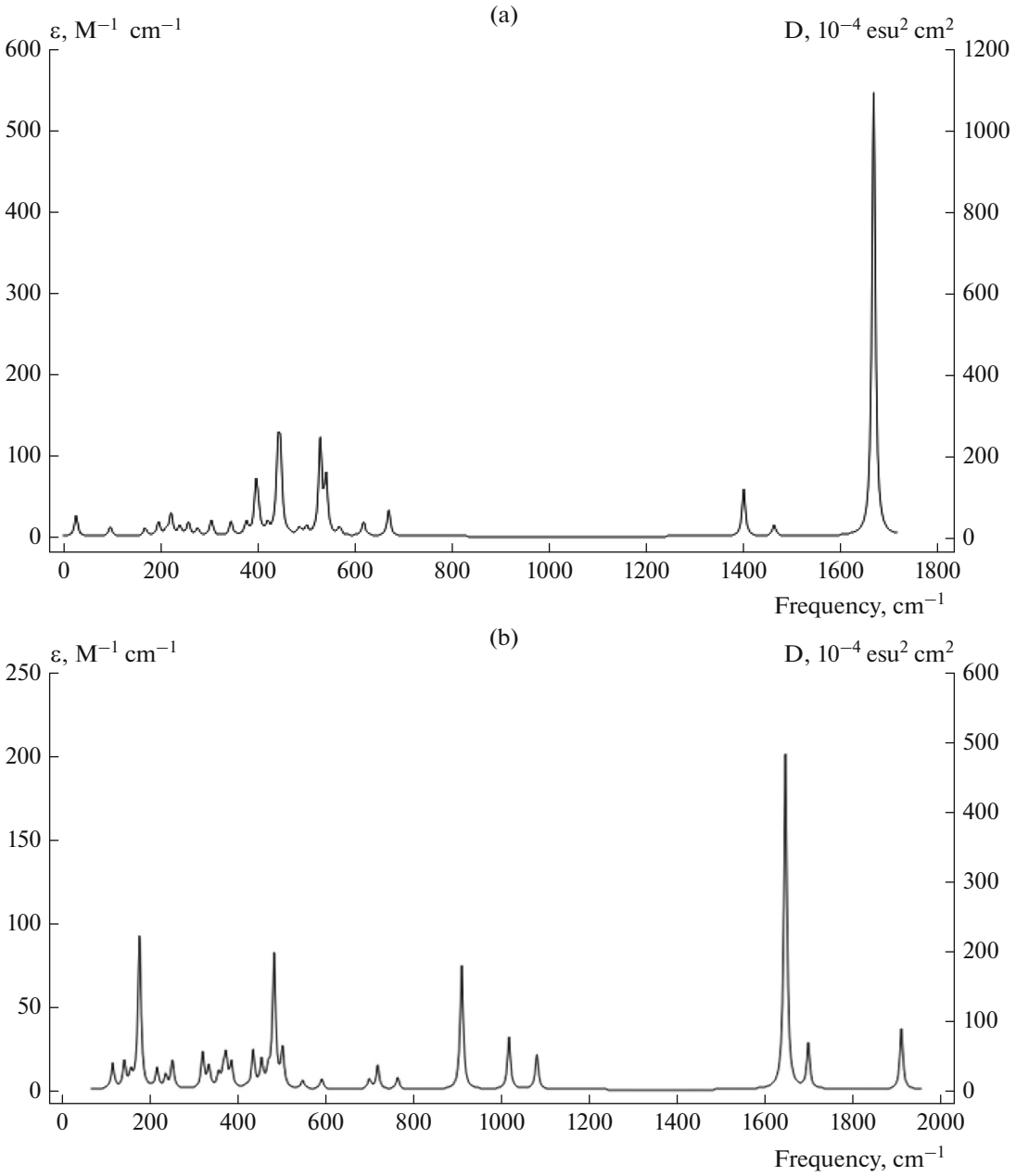

Fig. 6. The frequency (cm^{-1}) changes through the IR spectra for (a) H_2@ B_5N_{10}_NC, (b) H_2@Al–B_4N_{10}_NC, (c) H_2@C–B_4N_{10}_NC, and (d) H_2@Si–B_4N_{10}_NC complexes using CAM–B3LYP–D3/6-311 + G (*d*, *p*), LANL2DZ [Note: ε (M^{-1} cm^{-1}) is the absorbance unit and D (10^{-4} esu^2 cm^2) is the dipole strength via the esu or electrostatic unit, which is a unit of charge in the cgs (centimeter-gram-second system)].

CONCLUSIONS

This investigation has discovered doping of X (X = Al, C, Si) elements on the boron nitride nanocell (B_5N_{10}_NC) for enhancing H_2 sensing applying in the hydrogen-based energy storage technology. Therefore, H_2 molecules adsorption involving the X–B_4N_{10}_NC has been experimented based on electrostatic interactions between the H_2 molecules and X–B_4N_{10}_NC complexes.

The electromagnetic and thermodynamic properties of X–B_4N_{10}_NC complexes were computed using density functional theory. The results have illustrated that chosen hydrogen molecules adsorbed on the X–B_4N_{10}_NC are rather stable with the most stable

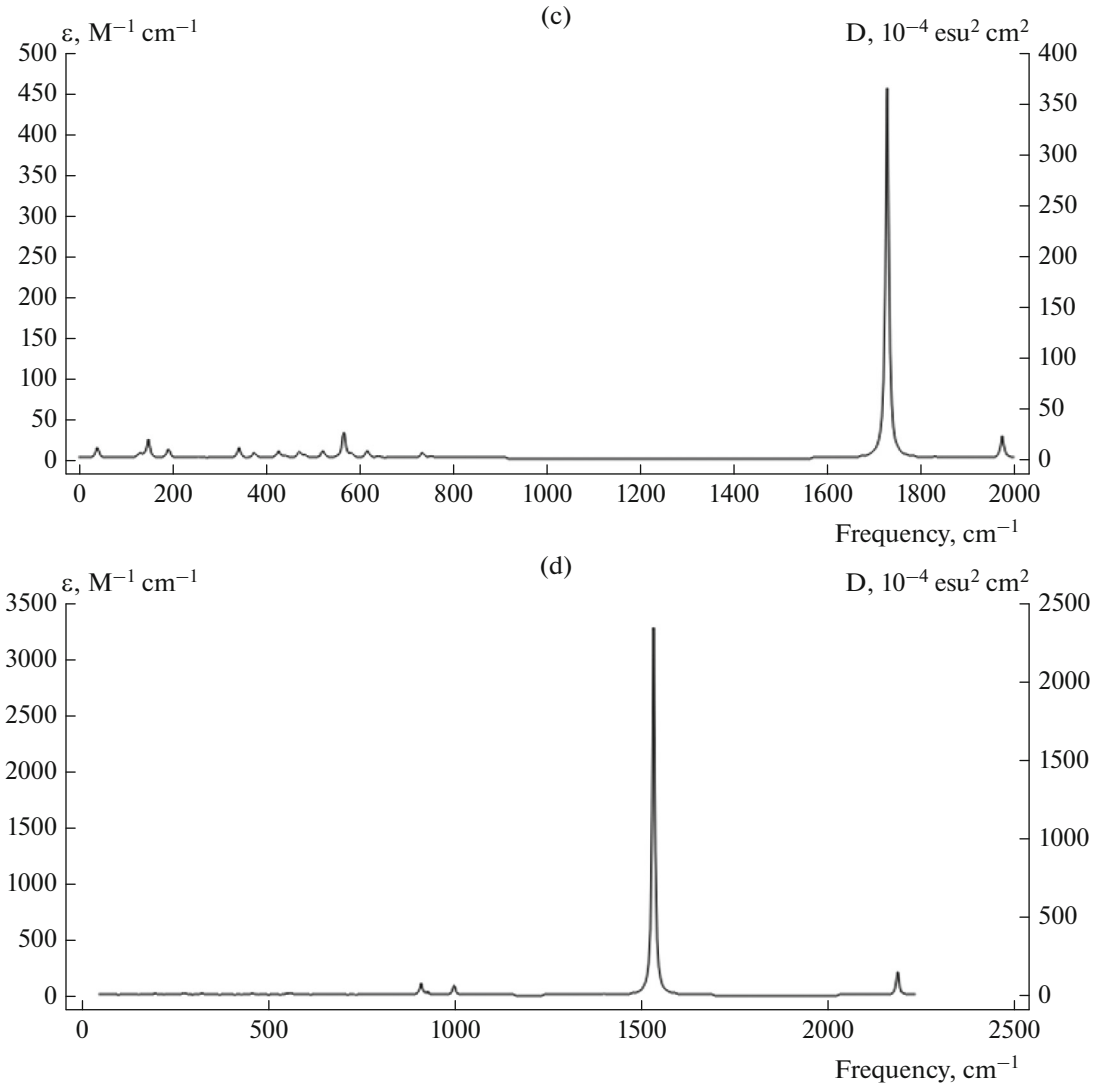

Fig. 6. (Contd.)

adsorption site being in the center of X–B_4N_{10}_NC system. The selectivity of atom-doped on boron nitride nanocell (hydrogen sensor) for H_2 molecules adsorption can be resulted as: H_2@Si–B_4N_{10}_NC > H_2@Al–B_4N_{10}_NC ≫ H_2@C–B_4N_{10}_NC complexes, respectively. As revealed by DFT-based analysis, the potency of X–B_4N_{10}_NC for grabbing H_2 molecules was determined mainly by the electronegativity of the functional groups, as well as the interaction between the X–B_4N_{10}_NC and the H_2 molecules.

ACKNOWLEDGMENTS

In successfully completing this paper and its research, the author is grateful to Kastamonu University.

FUNDING

This work was supported by ongoing institutional funding. No additional grants to carry out or direct this particular research were obtained.

CONFLICT OF INTEREST

The author of this work declares that he has no conflicts of interest.

REFERENCES

1. H. Ran, J. Yin, and H. Li, Nanomaterials **13**, 584 (2023). https://doi.org/10.3390/nano13030584
2. D. V. Shtansky, A. T. Matveev, E. S. Permyakova, et al., Nanomaterials **12**, 2810 (2022). https://doi.org/10.3390/nano12162810

3. E. A. Lebedeva, S. A. Astaf'eva, and T. S. Istomina, Russ. J. Phys. Chem. B **16**, 316–322 (2022). https://doi.org/10.1134/S1990793122010109
4. F. Mollaamin and M. Monajjemi, J. Mol. Struct. **1300**, 137214 (2024). https://doi.org/10.1016/j.molstruc.2023.137214
5. D. V. Shtansky, A. T. Matveev, E. S. Permyakova, et al., Nanomaterials **12**, 2810 (2022). https://doi.org/10.3390/nano12162810
6. Y. Yang, Y. Peng, M. F. Saleem, et al., Materials **15**, 4396 (2022). https://doi.org/10.3390/ma15134396
7. A. Davies, J. D. Albar, A. Summerfield, et al., Nano Lett. **18**, 498–504 (2018). https://doi.org/10.1021/acs.nanolett.7b04453
8. R. S. Bangari, V. K. Yadav, J. K. Singh, et al., ACS Omega **5**, 10301–10314 (2020). https://doi.org/10.1021/acsomega.9b04295
9. Y. H. Chao, J. Zhang, H. P. Li, et al., Chem. Eng. J. **387**, 124138 (2020). https://doi.org/10.1016/j.cej.2020.124138
10. V. Vatanpour, S. A. N. Mehrabani, B. Keskin, et al., Ind. Eng. Chem. Res. **60**, 13391–13424 (2021). https://doi.org/10.1021/acs.iecr.1c02102
11. N. V. Dokhlikova, S. A. Ozerin, S. V. Doronin, et al., Russ. J. Phys. Chem. B **16**, 461–467 (2022). https://doi.org/10.1134/S1990793122030137
12. Y. Guo, R. X. Wang, P. F. Wang, et al., ACS Sustain. Chem. **7**, 5727–5741 (2019). https://doi.org/10.1021/ACSSUSCHEMENG.8B05150
13. M. I. Ikim, E. Y. Spiridonova, V. F. Gromov, et al., Russ. J. Phys. Chem. B **17**, 774–777 (2023). https://doi.org/10.1134/S199079312303003X
14. N. V. Dokhlikova, A. K. Gatin, S. Y. Sarvadiy, et al., J. Phys. Chem. B **16**, 361–369 (2022). https://doi.org/10.1134/S1990793122020166
15. K. Y. Troshin, N. M. Rubtsov, G. I. Tsvetkov, et al., Russ. J. Phys. Chem. B **17**, 979–985 (2023). https://doi.org/10.1134/S1990793123040310
16. M. A. Qyyum, Y. D. Chaniago, W. Ali, et al., Energies **13**, 5023 (2020). https://doi.org/10.3390/en13195023
17. E. I. Rudenko, N. V. Dohlikova, A. K. Gatin, et al., Russ. J. Phys. Chem. B **17**, 845–852 (2023). https://doi.org/10.1134/S1990793123040164
18. A. M. Tereza, G. L. Agafonov, E. K. Anderzhanov, et al., Russ. J. Phys. Chem. B **17**, 974–978 (2023). https://doi.org/10.1134/S1990793123040309
19. M. A. Kotov, S. Y. Lavrentyev, N. G. Solovyov, et al., Russ. J. Phys. Chem. B **17**, 953–961 (2023). https://doi.org/10.1134/S1990793123040267
20. E. Rivard, M. Trudeau, and K. Zaghib, Materials **12**, 1973 (2019). https://doi.org/10.3390/ma12121973
21. S. N. Kozlov and B. E. Zhestkov, Russ. J. Phys. Chem. B **16**, 1030–1037 (2022). https://doi.org/10.1134/S1990793122060069
22. A. M. Kuperman, A. Y. Sergeev, R. A. Turusov, et al., Russ. J. Phys. Chem. B **16**, 1172–1179 (2022). https://doi.org/10.1134/S1990793122060070
23. K. Y. Troshin, N. M. Rubtsov, G. I. Tsvetkov, et al., Russ. J. Phys. Chem. B **16**, 693–698 (2022). https://doi.org/10.1134/S1990793122040303
24. N. V. Dokhlikova, A. K. Gatin, S. Y. Sarvadiy, et al., Russ. J. Phys. Chem. B **16**, 772–779 (2022). https://doi.org/10.1134/S1990793122040042
25. L. I. Trakhtenberg, Russ. J. Phys. Chem. B **17**, 600–607 (2023). https://doi.org/10.1134/S1990793123030144
26. F. Mollaamin and M. Monajjemi, Russ. J. Phys. Chem. B **17**, 658–672 (2023). https://doi.org/10.1134/S1990793123030223
27. M. G., Kucherenko, P. P. Neyasov, and N. Y. Kruchinin, Russ. J. Phys. Chem. B **17**, 745–754 (2023). https://doi.org/10.1134/S1990793123030053
28. F. Mollaamin and M. Monajjemi, Sensor Rev. **43**, 266–279 (2023). https://doi.org/10.1108/SR-03-2023-0040
29. I. S. Golyak, D. R. Anfimov, I. B. Vintaykin, et al., Russ. J. Phys. Chem. B **17**, 320–328 (2023). https://doi.org/10.1134/S1990793123020264
30. F. Mollaamin and M. Monajjemi, J. Mol. Model. **29**, 170 (2023). https://doi.org/10.1007/s00894-023-05567-8
31. M. M. Avilova, N. V. Zolotareva, and O. V. Popova, Russ. J. Phys. Chem. B **17**, 329–335 (2023). https://doi.org/10.1134/S1990793123020203
32. M. Monajjemi, F. Mollaamin, and S. Shojaei, Biointerface Res. Appl. Chem. **10**, 5575 (2020). https://doi.org/10.33263/BRIAC103.575585
33. S. Shahriari, F. Mollaamin, and M. Monajjemi, Micromachines **14**, 241 (2023). https://doi.org/10.3390/mi14020241
34. F. Mollaamin, A. Ilkhani, N. Sakhaei, et al., J. Comput. Theor. Nanosci. **12**, 3148–3154 (2015). https://doi.org/10.1166/jctn.2015.4092
35. B. Khalili Hadad, F. Mollaamin, and M. Monajjemi, Russ. Chem. Bull. **60**, 238–241 (2011). https://doi.org/10.1007/s11172-011-0039-5
36. M. Monajjemi, L. Mahdavian, F. Mollaamin, et al., Russ. J. Inorg. Chem. **54**, 1465–1473 (2009). https://doi.org/10.1134/S0036023609090216
37. A. Tahan, F. Mollaamin, and M. Monajjemi, Russ. J. Phys. Chem. **83**, 587–597 (2009). https://doi.org/10.1134/S003602440904013X
38. M. Monajjemi, M. T. Baie, and F. Mollaamin, Russ. Chem. Bull. **59**, 886–889 (2010). https://doi.org/10.1007/s11172-010-0181-5
39. S. Shahriari, M. Monajjemi, and F. Mollaamin, J. Chil. Chem. Soc. **67**, 5468–5476 (2022). https://doi.org/10.4067/S0717-97072022000205468
40. M. A. A. Zadeh, H. Lari, L. Kharghanian, et al., J. Comput. Theor. Nanosci. **12**, 4358 (2015). https://doi.org/10.1166/jctn.2015.4366
41. E. M. Sarasia, S. Afsharnezhad, B. Honarparvar, et al., Phys. Chem. Liq. **49**, 561–571 (2011). https://doi.org/10.1080/00319101003698992
42. S. Shahriari, M. Monajjemi, and K. Zare, Biointerface Res. Appl. Chem. **8**, 3219–3223 (2018)
43. M. Khaleghian, M. Zahmatkesh, F. Mollaamin, et al., Fuller. Nanotub. Carbon Nanostruct. **19**, 251–261

(2011).
https://doi.org/10.1080/15363831003721757

44. F. Mollaamin and M. Monajjemi, J. Comput. Theor. Nanosci. **12**, 1030–1039 (2015).
https://doi.org/10.1166/jctn.2015.3846

45. K. Bakhshi, F. Mollaamin, and M. Monajjemi, J. Comput. Theor. Nanosci. **8**, 763–768 (2011).
https://doi.org/10.1166/jctn.2011.1750

46. F. Mollaamin, M. Monajjemi, S. Salemi, et al., Fuller. Nanotub. Carbon Nanostruct. **19**, 182 (2011).
https://doi.org/10.1080/15363831003782932

47. M. Monajjemi, M. Khaleghian, N. Tadayonpour, et al., Int. J. Nanosci. **9**, 517–529 (2010).
https://doi.org/10.1142/S0219581X10007071

48. A. H. Davtyan, Z. O. Manukyan, S. D. Arsentev, et al., Russ. J. Phys. Chem. B **17**, 336–345 (2023).
https://doi.org/10.1134/S1990793123020239

49. K. Y. Troshin, N. M. Rubtsov, G. I. Tsvetkov, et al., Russ. J. Phys. Chem. B **17**, 433–438 (2023).
https://doi.org/10.1134/S1990793123020185

50. F. Mollaamin and M. Monajjemi, J. Clust. Sci. **34**, 2901 (2023).
https://doi.org/10.1007/s10876-023-02436-5

51. F. Mollaamin and M. Monajjemi, J. Mol. Model. **29**, 119 (2023).
https://doi.org/10.1007/s00894-023-05526-3

52. J. P. Perdew, K. Burke, and M. Ernzerhof, Phys. Rev. Lett. **77**, 3865 (1996).
https://doi.org/10.1103/PhysRevLett.77.3865

53. R. Alaya, K. Kourchid, Y. Althaqafi, et al., Russ. J. Phys. Chem. B **17**, 868–877 (2023).
https://doi.org/10.1134/S1990793123040024

54. X. Yuan, X. Tan, and B. Liu, Russ. J. Phys. Chem. B **17**, 886–895 (2023).
https://doi.org/10.1134/S1990793123040322

55. P. Hohenberg and W. Kohn, Phys. Rev. B **136**, B864–B871 (1964).
https://doi.org/10.1103/PhysRev.136.B864

56. W. Kohn and L. J. Sham, Phys. Rev. **140**, A1133–A1138 (1965).
https://doi.org/10.1103/PhysRev.140.A1133

57. A. D. Becke, J. Chem. Phys. **98**, 5648–5652 (1993).
https://doi.org/10.1063/1.464913

58. C. Lee, W. Yang, and R. G. Parr, Phys. Rev. B **37**, 785–789 (1988).
https://doi.org/10.1103/PhysRevB.37.785

59. K. Kim and K. D. Jordan, J. Phys. Chem. **98**, 10089–10094 (1994).
https://doi.org/10.1021/j100091a024

60. P. J. Stephens, F. J. Devlin, C. F. Chabalowski, et al., J. Phys. Chem. **98**, 11623–11627 (1994).
https://doi.org/10.1021/j100096a001

61. C. J. Cramer, *Essentials of Computational Chemistry: Theories and Models*, 2nd ed. (Wiley, Hoboken, NJ, 2004).

62. F. Mollaamin and M. Monajjemi, Int. J. Quantum Chem. **124**, e27348 (2024).
https://doi.org/10.1002/qua.27348

63. F. Mollaamin and M. Monajjemi, Mol. Simul. **49**, 365 (2023).
https://doi.org/10.1080/08927022.2022.2159996

64. S. H. Touhami, K. Almi, S. Lakel, et al., Russ. J. Phys. Chem. B **17**, 1057–1068 (2023).
https://doi.org/10.1134/S1990793123050287

65. M. J. Frisch, G. W. Trucks, H. B. Schlegel, G. E. Scuseria, M. A. Robb, J. R. Cheeseman, G. Scalmani, V. Barone, G. A. Petersson, H. Nakatsuji, X. Li, M. Caricato, A. V. Marenich, J. Bloino, B. G. Janesko, R. Gomperts, B. Mennucci, H. P. Hratchian, J. V. Ortiz, A. F. Izmaylov, J. L. Sonnenberg, D. Williams-Young, F. Ding, F. Lipparini, F. Egidi, J. Goings, B. Peng, A. Petrone, T. Henderson, D. Ranasinghe, V. G. Zakrzewski, J. Gao, N. Rega, G. Zheng, W. Liang, M. Hada, M. Ehara, K. Toyota, R. Fukuda, J. Hasegawa, M. Ishida, T. Nakajima, Y. Honda, O. Kitao, H. Nakai, T. Vreven, K. Throssell, J. A. Montgomery, Jr., J. E. Peralta, F. Ogliaro, M. J. Bearpark, J. J. Heyd, E. N. Brothers, K. N. Kudin, V. N. Staroverov, T. A. Keith, R. Kobayashi, J. Normand, K. Raghavachari, A. P. Rendell, J. C. Burant, S. S. Iyengar, J. Tomasi, M. Cossi, J. M. Millam, M. Klene, C. Adamo, R. Cammi, J. W. Ochterski, R. L. Martin, K. Morokuma, O. Farkas, J. B. Foresman, and D. J. Fox, *Gaussian 16, Revision C.01* (Gaussian, Inc., Wallingford, CT, 2016).

66. R. Dennington, T. A. Keith, and J. M. Millam, *GaussView, Version 6.06.16* (Semichem Inc., Shawnee Mission, KS, 2016).

67. F. Mollaamin and M. Monajjemi, Computation **11**, 108 (2023).
https://doi.org/10.3390/computation11060108

68. F. Mollaamin and M. Monajjemi, C J. Carbon Res. **9**, 20 (2023).
https://doi.org/10.3390/c9010020

69. O. Poleshchuk, E. Kalinina, J. Latosińska, et al., J. Molec. Struct. (Theochem.) **547**, 233–243 (2001).
https://doi.org/10.1016/S0166-1280(01)00636-4

70. A. A. Shmyreva, V. E. Kirillov, E. B. Dzhangurazov, et al., Russ. J. Phys. Chem. B **17**, 764–773 (2023).
https://doi.org/10.1134/S1990793123030120

71. F. Mollaamin, S. Shahriari, M. Monajjemi, et al., J. Clust. Sci. **34**, 1547–1562 (2023).
https://doi.org/10.1007/s10876-022-02335-1

72. J. Li, S. He, W. Dai, et al., Mater. Technol. **35**, 691–696 (2020).
https://doi.org/10.1080/10667857.2017.1387718

73. G. Venkateswarlu, D. Madhu, and J. V. Rani, Mater. Chem. Phys. **226**, 356–361 (2019).
https://doi.org/10.1016/j.matchemphys.2019.01.051

74. W. Li, L. Jiang, W. Jiang, et al., J. Mater. Res. Technol. **26**, 2028–2042 (2023).
https://doi.org/10.1016/j.jmrt.2023.08.035